Sparse 2D SAR Apertures for 3D SAR and Tomogram Image Formation

Dr. Daniel Andre
Centre for Electronic Warfare Information and Cyber,
Cranfield University,
Defence Academy of the United Kingdom,
Shrivenham
SN6 8LA
UNITED KINGDOM
d.andre@cranfield.ac.uk

George A J Price
QinetiQ, Malvern Technology Centre
St. Andrews Road
Malvern
WR14 1ET
UNITED KINGDOM
gaprice@qinetiq.com

Dr. Mark Finnis
Centre for Defence Engineering,
Cranfield University,
Defence Academy of the United Kingdom,
Shrivenham
SN6 8LA
UNITED KINGDOM
m.v.finnis@cranfield.ac.uk

Prof David Blacknell
Dstl,
Porton Down,
Salisbury,
SP4 0JQ
UNITED KINGDOM
dblacknell@dstl.gov.uk

ABSTRACT

Remotely sensed three-dimensional Synthetic Aperture Radar (SAR) images, or more basic two-dimensional tomogram SAR images, have the potential to provide useful intelligence for different scenarios, assisting in object recognition and eliminating the radar layover effects that can confuse and clutter imagery. One such important scenario is through-wall low frequency SAR remote sensing into buildings. Projection due to features on ceilings, multiple floors and roofs can severely clutter conventional two-dimensional SAR images, whereas this projective clutter does not impact three-dimensional images: the clutter signatures are formed at their correct heights and away from the three-dimensional region of interest. As promising as this imaging technique would seem, the full two-dimensional aperture sampling technique is highly data intensive, requiring radar collections finely sampled in both azimuth and elevation angles. The purpose of this research is to investigate practical sparse sampled two-dimensional SAR collections with the intention of substantially reducing the sampling required whilst still maintaining a useful result. This would be achieved through the reduction of sidelobe levels and aliasing effects. This work extends previous sparse sampled three-dimensional SAR imaging simulation based investigations to full scale radar measurements at the Cranfield Ground-Based SAR Laboratory and is undertaken as part of the Dstl Remote Intelligence of Building Interiors research programme.

1.0 INTRODUCTION

Remotely sensed three-dimensional Synthetic Aperture Radar (SAR) images have the potential to provide useful intelligence for different scenarios, assisting in object recognition and eliminating the radar layover effects that can confuse and clutter imagery. One such important scenario is through-wall low frequency SAR remote sensing into buildings. Projection due to features on ceilings, multiple floors and roofs can severely clutter conventional two-dimensional SAR images, whereas this projective clutter does not impact the three-dimensional images: the clutter signatures are formed at their correct heights and away from the three-dimensional region of interest

Although this sensing technique could have great utility, the full two-dimensional aperture sampling technique is highly data intensive, requiring radar collections finely sampled in both azimuth and elevation angles. The purpose of the research presented here is to investigate more practical sparse sampled two-dimensional SAR collections which are faster to collect with the intention of substantially reducing the sampling required whilst providing a useful result. This would be achieved through the reduction or control of sidelobe levels and aliasing effects. Some of the proposed trajectories involve multiple nonlinear flybys,

and it is envisaged that some of these trajectories may be practical for emerging drone based multistatic radar swarms for example.

This work extends previous sparse sampled three-dimensional SAR imaging based investigations [1-2] to full scale radar measurements at the Cranfield Ground-Based SAR Laboratory and is undertaken as part of the Dstl Remote Intelligence of Building Interiors research programme.

2.0 THE MEASURED SCENE

2D SAR aperture data was collected with the GBSAR system based at Cranfield University. The GBSAR system is a rail-mounted radar capable of operating at a wide range of frequencies with a precise positioning solution. This allows for well-controlled collections and thus a relatively simple case for processing and algorithm development. Figure 1 shows the radar laboratory setup for the data analysed here. Figure 1a shows the behind wall scene, and the scanning system us visible on the other side. The wall is made of concrete bricks. The scene from the radar point of view can be seen in Figure 1b.

The sensed frequency range was 1-6 GHz and the 2D SAR aperture had vertical by horizontal dimensions of 1.5 by 3.5m respectively, with 2cm spacing in each dimension. The 5GHz bandwidth provides a 3cm range resolution, whilst the resolution in azimuth and elevation cross-ranges is variable due to the SAR-nearfield measurement regime. At a range of 4m the azimuth and elevation cross-range resolutions are approximately 5cm and 12cm respectively. The dataset presented is HH polarized and monostatic.

When all of collected data is input into the three-dimensional backprojection image formation algorithm, a volumetric SAR image is generated. A rendering of the image is presented in Figure 1c. Here, no laboratory background subtraction was necessary, as the various clutter sources have been imaged to their correct locations in three-dimensions, leaving the scene clear apart from some sidelobe artefacts. The corrugated back wall of the laboratory is clearly visible, and the top and bottom of the concrete wall is visible in the centre. Some of the items hidden behind the wall can be seen in this rendering. It is noted that at no point in the two-dimensional SAR aperture, is there a wall-free line of site to any of the objects of interest place in the scene: monitor, desk, computer, briefcase and barrels.

It can be difficult to present volumetric data in a clear and concise manner. In the remainder of this paper, orthogonal axis projections of the region of interest of volumetric SAR images are presented, allowing the comparison of image quality as a function of sparse collection trajectory.

Figure 2a shows orthogonal projections from the region of interest, taken from the volumetric image of Figure 1c, from left to right with side, front and plan projection views, z being the vertical axis, x being aligned with the rail, and y being aligned with the range direction. The radar scanning rail itself is located at the positive-*y* extreme of the images. The transceiver positioning in the image coordinate system can be seen more precisely in Figure 3a.

Once again, the top and bottom of the wall are the most prominent features. To simplify the ensuing analysis the wall scattering itself has been subtracted from the data, by means of a background scan subtraction, more clearly revealing the objects behind, as seen in Figure 2b. The most prominent objects visible are the monitor on the desk, the base of the metal briefcase, the base of the two barrels, and the multipath artefact from between the two barrels. To a lesser extent the leading edge of the desk itself is visible, as is the extent of the briefcase in height, and the leading edge of the barrels. For the remainder of the sparse aperture analysis, the background subtracted dataset will be employed.


a)

b)

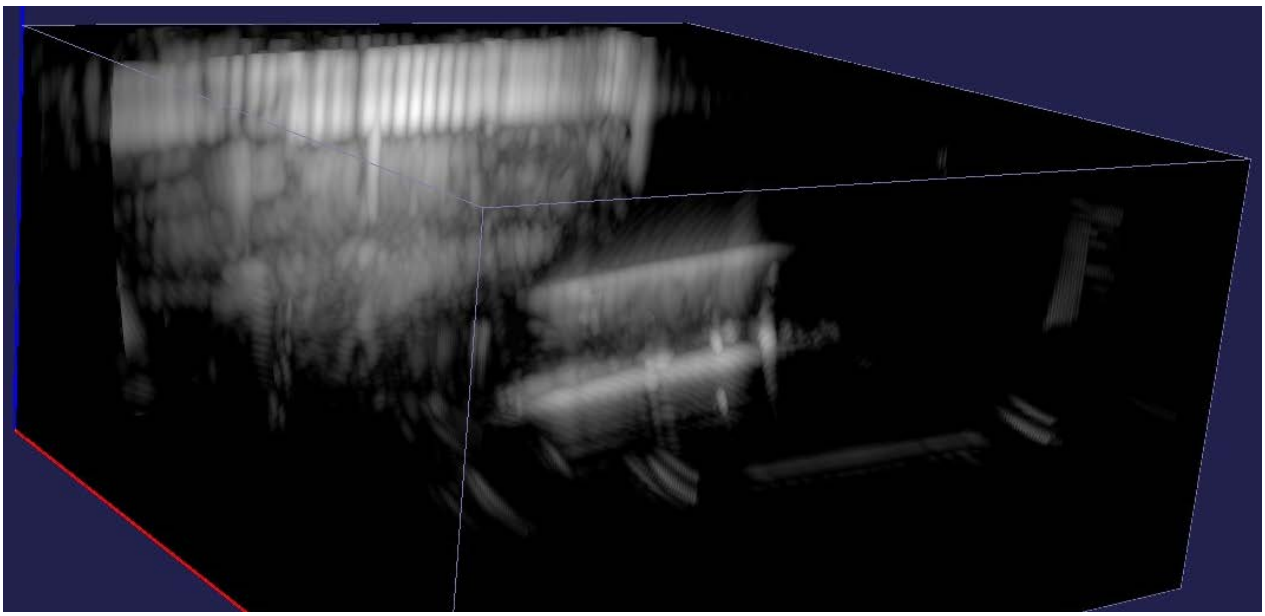
c)

Figure 1: The through-wall measured scene. The behind wall scene consists of six items with the radar scanning rail visible in the background (a); the radar point of view of the scene shows the occluding concrete wall (b); a rendering of the fully sampled volumetric SAR image with the region of interest in centre (c).

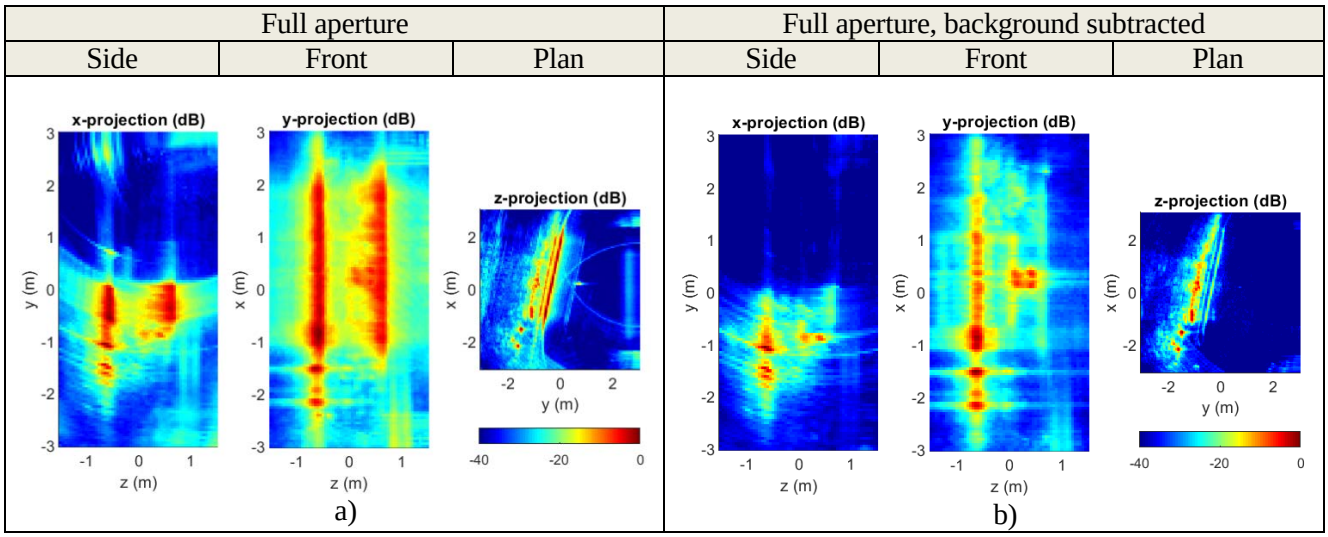

Figure 2: Orthogonal projections of fully sampled volumetric SAR images centred on the region of interest. The original dataset (also shown in Figure1c) shows a strong wall response (a); the background subtracted volumetric SAR projection (b) has wall response mostly removed bringing the through-wall scene into prominence.

3.0 SPARSE TRAJECTORIES

3.1 Classes of Sparse Trajectories Investigated and Approach

In order to investigate faster, simpler and thus more practical volumetric SAR collection strategies, numerous sparsely sampled two-dimensional SAR apertures were investigated. In this paper we only describe results from five classes of sparse trajectory which help characterise the principle artefacting effects, these are shown in Figure 3 – for comparison, the fully sampled two-dimensional SAR aperture is shown in Figure 3a. The GBSAR system has separate antennas for transmission and reception, and in the trajectory figures the transmission points are coloured red, and the reception points are coloured blue. The antenna separation is 22.7cm and the image formation algorithm is bistatic, however we refer to the dataset as monostatic.

The five classes of sparse trajectories described here are:

- Repeat linear passes at evenly spaced heights, (sparse-RL), Figure 3b;
- Repeat linear passes at non-linearly spaced heights, (sparse-RL-NLH), Figure 3c;
- Crossing linear trajectories, (sparse-CL), Figure 3d;
- Crossing sinusoidal trajectories, (sparse-CS), Figure 3e;
- Non-overlapping repeat pass sinusoidal trajectories at different heights, (sparse-RS), Figure 3f.

Within the classes the number of passes or crosses were varied. For example the number of repeat passes investigated in the sparse-RL class varied from 2 to 78.

Rather than resetting the GBSAR system to actually run these various sparse trajectories, the investigative approach was to obtain the corresponding sparsely sampled radar data through interpolation from the measured fully sampled radar dataset.

2.2 Linear Repeat Pass Trajectories

The results for the Sparse-RL trajectories can be seen in Figure 4a-c. Figure 4a shows the result from two linear passes, and no vertical resolution is discernible, with the scatterer responses smeared across all heights. With four linear passes, it is now possible to just make out a few of the scatterers in the vertical dimension, and with twelve passes, in Figure 4c they are now clearly visible at their correct heights. The drawback with Sparse-RL however is that significant aliasing artefacts are present. The basic trend with increasing linear passes is that the separation between the scatterers and the corresponding aliased artefacts increases. Basic considerations show that the theoretical relation between the number of passes N_z and the aliasing separation L_z is approximately:

$$N_z = \frac{2 f_c A_z}{cR} L_z + 1 \tag{1}$$

Where f_c is the centre frequency, A_z is the vertical aperture length, c is the speed of light and R is the range. Equation (1) accounts for the bulk of the aliased energy, however if one wishes to make sure that absolutely all the aliased energy is accounted for, the maximum frequency can be used in the formula instead. Thus given a range of 4m, vertical aperture of 1.5m and centre frequency of 3.5GHz we have that 12 passes gives an aliasing separation of 1.26m which agrees with the result in Figure 4c. It is estimated that for the bulk of aliasing artefacts to be ejected from the image, 24 passes would be required.

In practice however, because the aliased features are spread out it was observed that 32 passes were required, this corresponding to a 4.6cm vertical spacing on the GBSAR rail – note that the actual spacing employed was 2cm. It is noted that if the maximum frequency were used in (1) then about 34 passes should be required to eliminate all artefacts, which is in agreement with measurement observation.

3.3 Linear Repeat Pass Trajectories Nonlinearly Separated in Height

Another approach briefly investigated was to nonlinearly distribute the linear trajectories in height, Sparse-RL-NLH, the intention being to smear out the aliased artefacts and thus reduce their maximum brightness. The sparse trajectory shown in Figure 2c was used to generate the volumetric SAR projections in Figure 3d. The aliased artefacts were indeed smeared out and their associated maximum intensity was thus reduced. It is likely that more optimal, possibly near random, vertical nonlinear spaced trajectories would give improved results. One detrimental feature of this approach however, is that the scatterer features of interest are also smeared out, so that resolution is reduced.

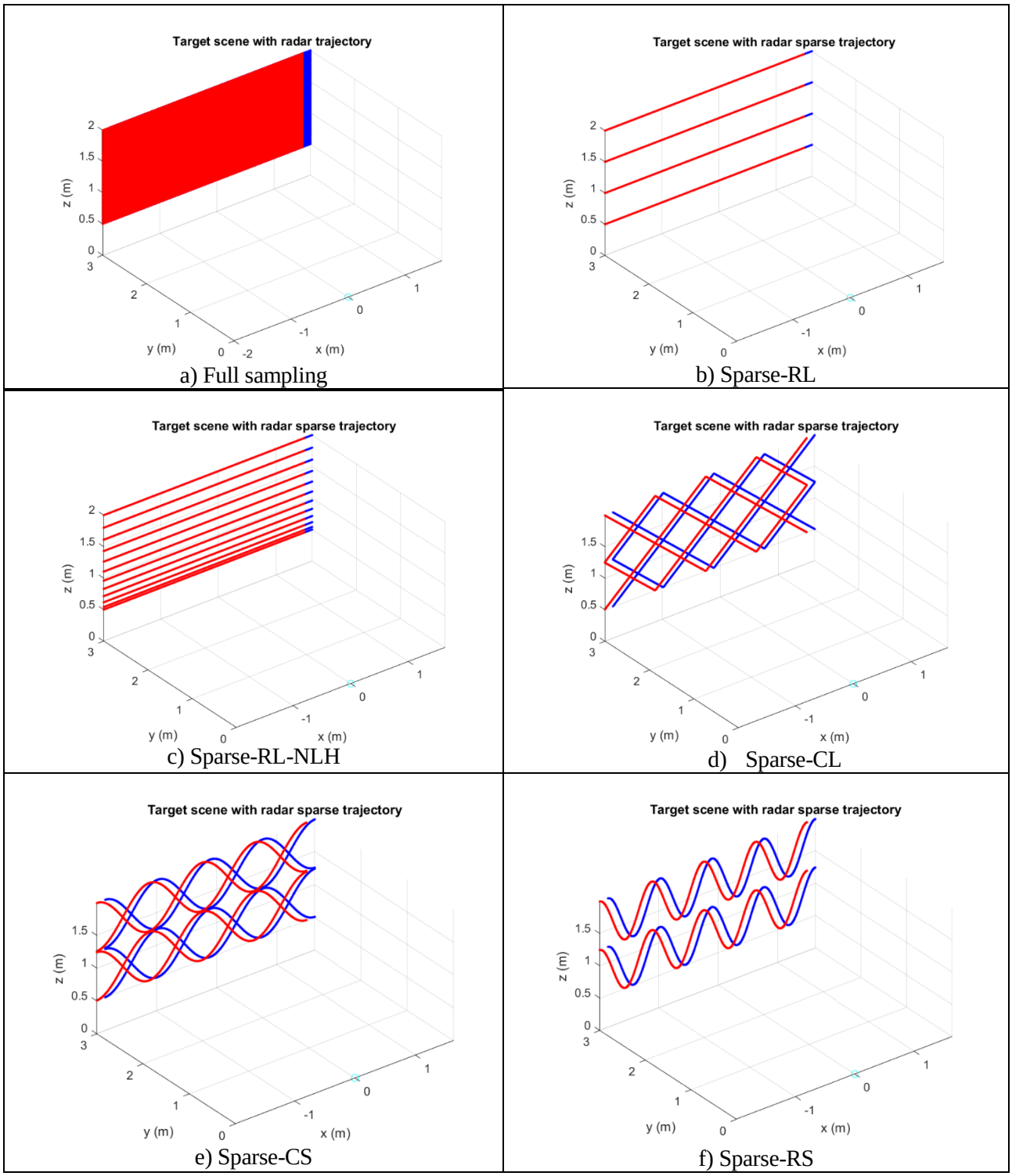

Figure 3: Two dimensional SAR aperture trajectories including fully sampled (a) and sparsely sampled classes of trajectory (b-f).

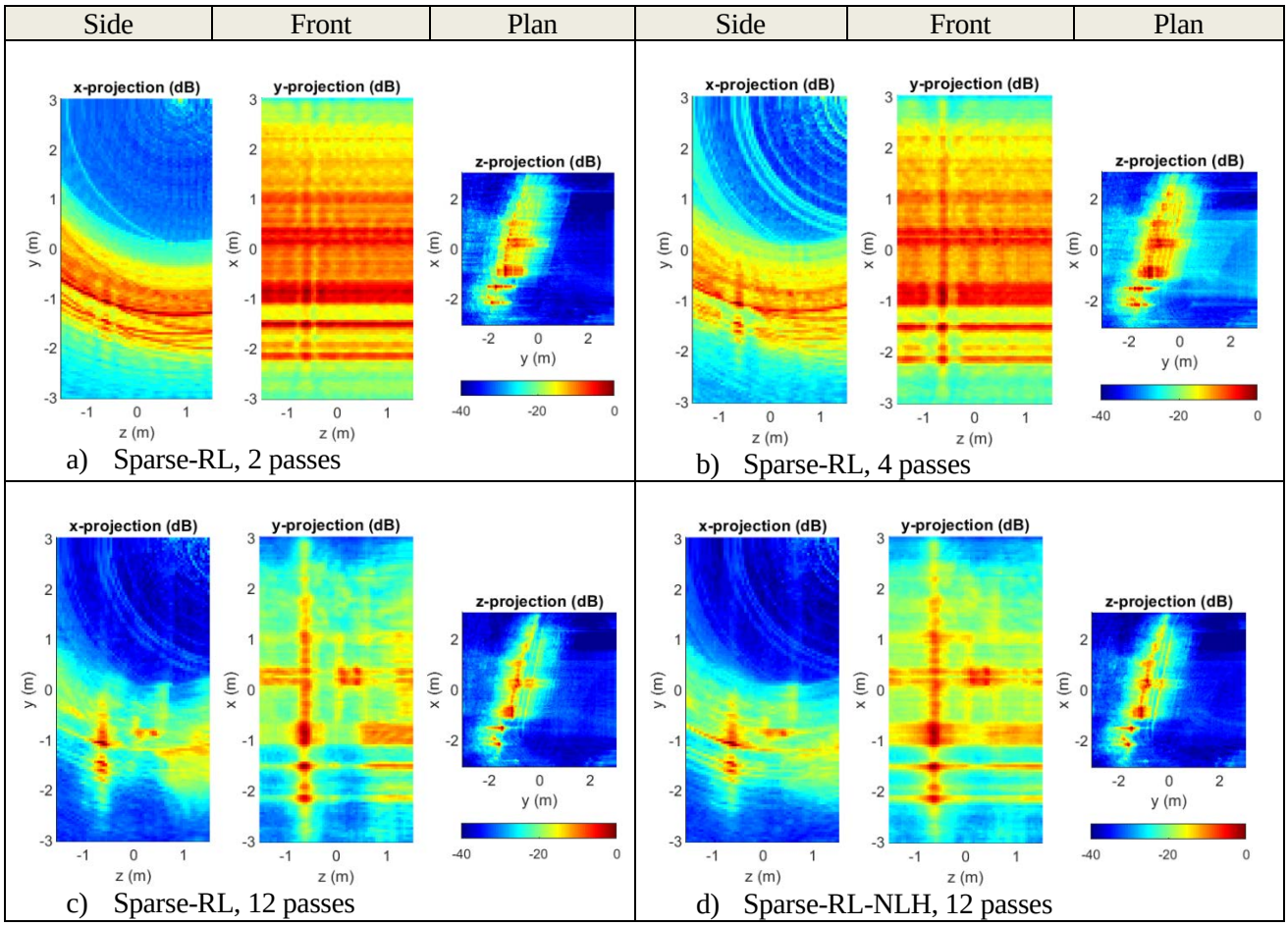

Figure 4: Orthogonal projections of background subtracted sparsely sampled volumetric SAR images centred on the region of interest. Sparse repeat linear trajectory results are shown with 2 pass (a), 4 pass (b), 12 pass (c) and nonlinearly distributed in height 12 pass (d).

3.4 Crossed trajectories

Crossed trajectories have been favoured for some three-dimensional SAR reconstructions, most notably the crossing nodes approach [3]. At the cross, effectively two coherent projections of the scene are generated, the coherence implying that the scene speckle matches between the two crossing trajectory legs. These two projections can be combined to provide either stereo vision, or as a means for automatic terrain height determination. This technique lends itself well to natural terrain surfaces which give rise to developed speckle.

Developing the crossing node concept, grids of crossed trajectories have here been investigated. The grids are composed of crosses, so for example that seen in Figure 3d is a 2 by 4 grid of crosses. This trajectory can also be thought of as a four horizontal-pass trajectory consisting of components zigzagging up and down.

The result from scanning with a single cross across the scene is shown in Figure 5a. This result can be thought of as the combination of two volumetric SAR images from straight line trajectories, each providing no resolution in different off-vertical curved axes, so that the scatterers are located where the ambiguous point spread functions cross each other. In the front y-projections, at these crossing points the scatterers are seen to give slightly elevated intensities, thus providing some three-dimensional localization. By searching for, or filtering for, these crosses one could envisage detecting scatterer locations in three-dimensions. Whilst in the front projection ambiguities in crossing location are present (as there are many lines crossing

throughout), it can be seen that some of this ambiguity is circumvented by consideration of the other two projections.

In a further attempt to lift the ambiguity, additional crosses are added to trajectories. Figure 5c shows the result from 1 by 2 crosses, still effectively 2 horizontal passes, and Figure 5e shows the result from 6 by 14 crosses, effectively 12 horizontal passes. In each case the scatterer locations are isolated successively more clearly. In the 12 pass case in Figure 5e the scatterer are well isolated however artefacting can be seen throughout the scene. These artefacts are again aliased artefacts however in diagonal directions due to the angle of the grid of trajectories. Basic considerations show that the theoretical relation between the number of horizontal passes N_z and the aliasing separation L_d is approximately

$$N_z = \frac{4f_c A_d}{cR} L_d \tag{1}$$

Where A_d is an effective diagonal aperture of approximately $1.5/\sqrt{2}=1.06$m, so that for 12 horizontal passes the diagonal aliasing distance is 0.97m, agreeing with Figure 5e. As before, the use of the centre frequency accounts for the bulk of the aliased energy, and one would use the maximum frequency to obtain the requirement for the removal of absolutely all aliased energy. For this class of trajectory, because the aliasing is diagonal, a greater aliasing distance is needed to eject the aliasing artefacts from the image when compared to the horizontal repeat pass trajectories. In practice about 46 horizontal zigzagging passes was required.

46 horizontal passes, are much more than the 32 horizontal passes required to eliminate the aliasing artefacts with the linear horizontal trajectories of the previous section. At first the crossing trajectories seem to be at a disadvantage but it should be recognized that for these, the aliased artefacts were at a lower dB level compared to the scattering centres. This is because the aliased energy has been more distributed across the image for the crossed trajectories. So if one is willing to reduce the volumetric image dynamic range, in some cases one can achieve superior results with relatively few crossed trajectories. Comparing Figure 4c and Figure 5e we see that for the same number of horizontal trajectories, the aliased artefacts are at a lower brightness for the crossed trajectories.

To further attempt to spread out and diminish the maximum brightness of the aliased energy, curved crossed trajectories, as seen in Figure 3e were next implemented, and the results corresponding to the linear crossed trajectories are presented in Figure 5b,d,f. The aliased energy has indeed been spread and smoothed out. This is most notable in the 2 by 4 cross example in Figure 5d. However with a higher number of crosses the curved crossing trajectory results are observed to converge with the linear crossing results.

It was observed that no artefacts remained in the scene when the grid of crosses was fine enough at 23 by 53 crosses, corresponding to 46 horizontal zigzagging paths. Here the vertical separation between zigzagging paths is 6.5cm and the shortest separation between the linear trajectories is 4.6cm, which is the same as the separation requirement observed for the repeat pass horizontal linear trajectories.

Sparse-CL			Sparse-CS		
Side	Front	Plan	Side	Front	Plan

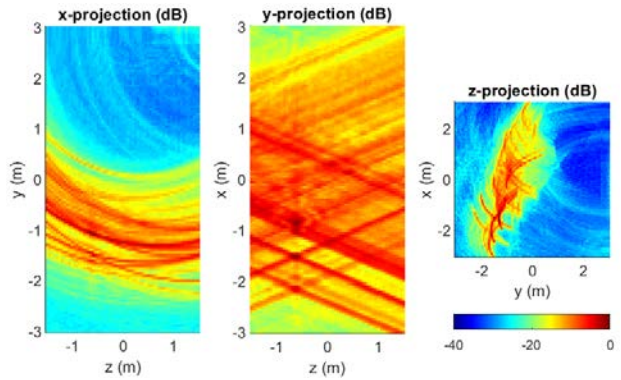

a) Sparse-CL, 2 passes, 1 cross

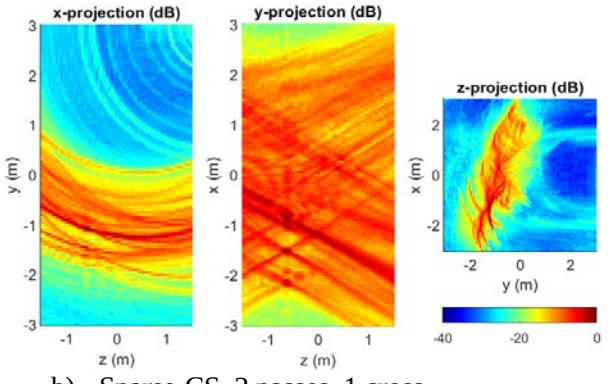

b) Sparse-CS, 2 passes, 1 cross

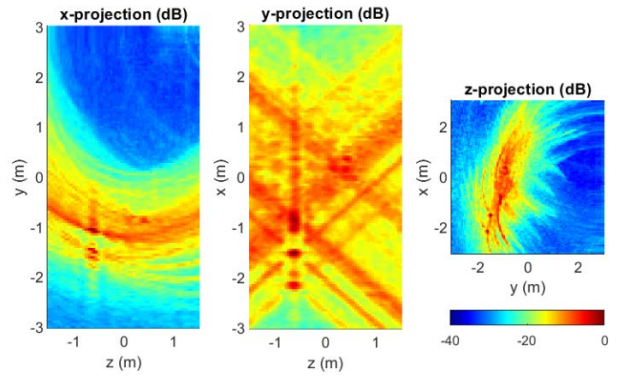

c) Sparse-CL, 4 passes, 2*4 crosses

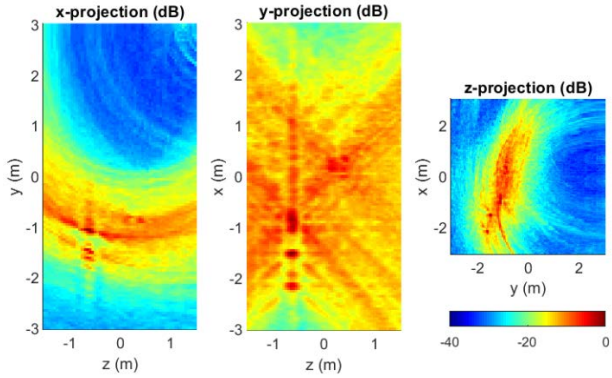

d) Sparse-CS, 4 passes, 2*4 crosses

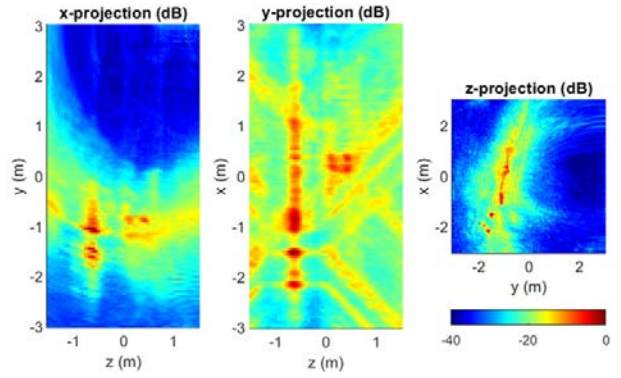

e) Sparse-CL, 12 passes, 6*14 crosses

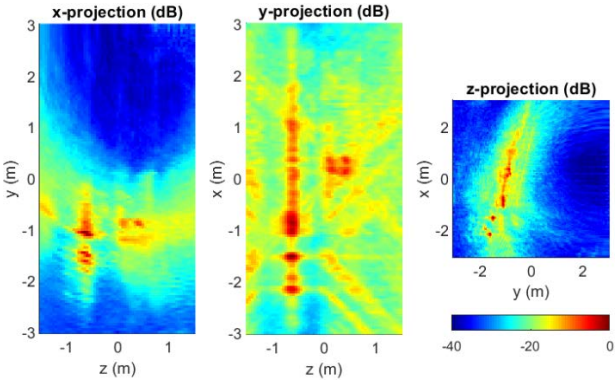

f) Sparse-CS, 12 passes, 6*14 crosses

Figure 5: Orthogonal projections of background subtracted sparsely sampled volumetric SAR images centred on the region of interest. Results for crossed linear trajectories are shown on the left and for curved trajectories, on the right. 2 pass results with one cross are shown in (a) and (b); 4 pass results with 2 by 4 crosses are shown in (c) and (d); 12 pass results with 6 by 14 crosses are shown in (e) and (f).

3.5 Sinusoid trajectories

Grids of crossing trajectories seem to lead to strong aliased artefacts. An approach to spreading these kinds of artefacts involves use of curved trajectories without crossings, as seen in Figure 3f. Results for 2, 3, 6 and 12 sinusoid passes are presented in Figure 6a-d. The horizontal sinusoid period distance is approximately equal to the vertical dimension of the oscillation of each sinusoid.

For the 2 pass trajectory in Figure 6a the aliased energy is substantially spread so that the scattering centre locations are just evident on the uniform background of aliased energy. The situation is further improved as more horizontal passes are added. Broadly speaking it could be said that the choice of number of horizontal sinusoid trajectories to use is dependent on the artefact free dynamic range required in the resultant image.

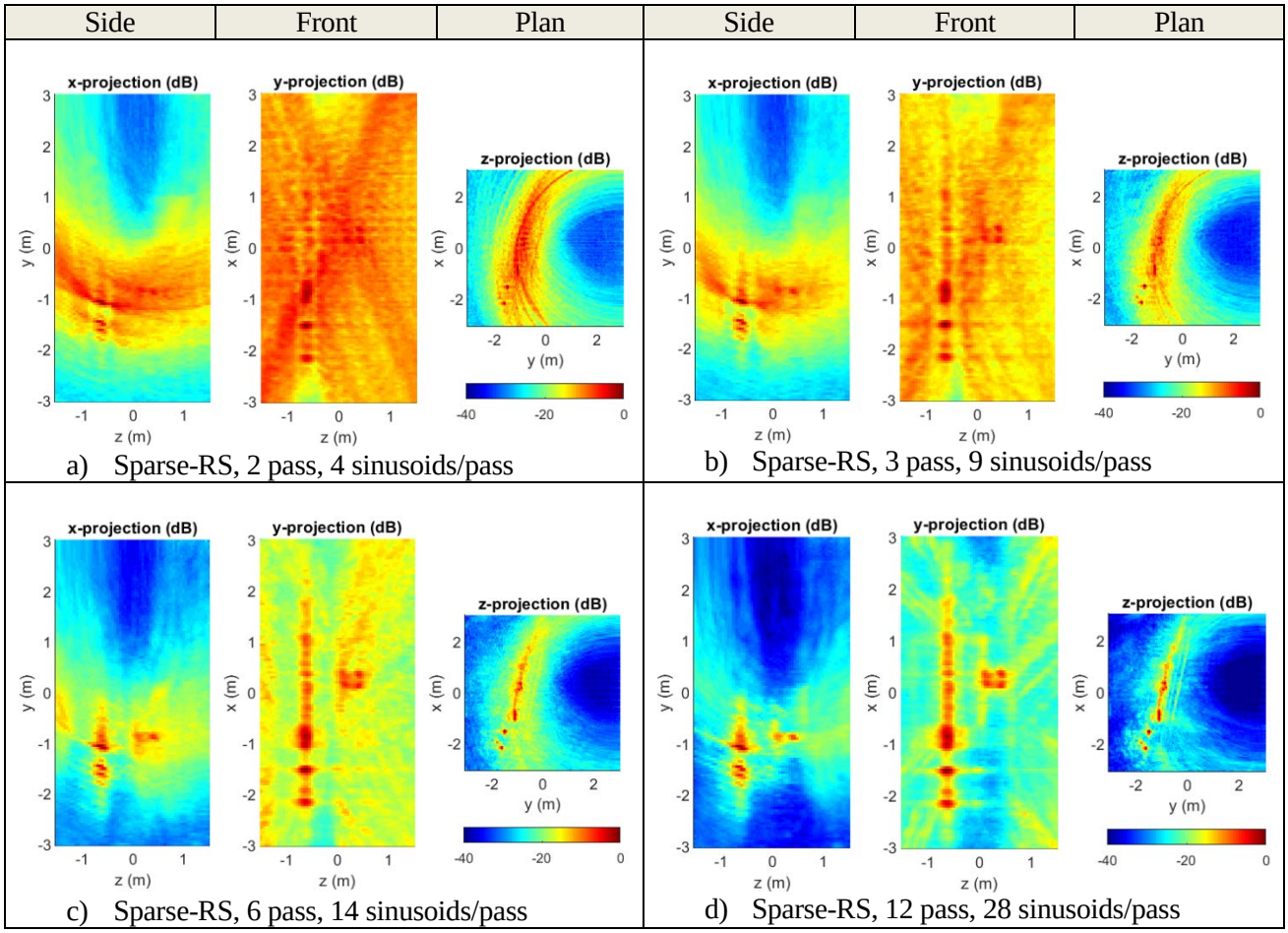

Figure 6: Orthogonal projections of background subtracted sparsely sampled volumetric SAR images centred on the region of interest. Results for crossed non-overlapping sinusoidal trajectories are presented with 2 pass (a); 3 pass (b); 6 pass (c) and 12 pass (d). The sinusoid period distance is approximately equal to the vertical dimension of each sinusoid.

For the 12 horizontal pass case, the vertical separation between passes is 13.6cm, giving rise to a dynamic range free from artefacts of approximately 15dB.

It was observed that no artefacts remained in the scene with about 24 sinusoid passes, which corresponds to a vertical separation of 6.3cm. The shortest distance between the sinusoids was about one third of this at 2.1cm

3.6 Results summary

For the classes of sparse trajectories investigated, the resolution can be thought of as mostly determined by the overall height and width extents of the trajectory ensemble, and the bulk of artefacts observed due to the sub-Nyquist sampling can be thought of as aliasing artefacts.

For the removal of sparse sampling artefacts in the scene, the observed number of repeat passes required for the principle classes of sparse trajectory and their separations are given in Table 1. Effectively these classes of trajectory will have achieved close-to-Nyquist sampling with these parameters.

Table 1: Number of repeat pass trajectories and their separations for the ejection of aliased artefacts for the principle sparse trajectories investigated.

	Pass number for artefact ejection	Vertical trajectory separation (cm)	Shortest trajectory separation (cm)
Sparse-RL	32	4.8	4.8
Sparse-CL	46 (23 by 53 crosses)	6.5	4.6
Sparse-RS	24 (56 sinusoids / pass)	6.3	2.1

It was found however that some sparse trajectories spread out the aliased energy, thus allowing an artefact free dynamic range even with a low number of sparse trajectories. Crossing linear and curved trajectories lowered the maximum intensity of aliased artefacts, however the repeat pass sinusoid trajectory spread the aliased energy out most evenly. For the repeat pass sinusoid trajectories, the trend observed was that the higher the density of trajectories, the wider the artefact free dynamic range.

For the GBSAR dataset an artefact free dynamic range of approximately 15dB required 12 sinusoid trajectory passes, so that the vertical separation of passes is 12.5cm, which is substantially less than the 4.8cm separation required for the same or greater artefact free dynamic range with 32 repeat horizontal linear passes.

4.0 CONCLUSION

Low frequency three-dimensional volumetric SAR imagery have advantages over conventional two-dimensional SAR imagery for the determination of the contents of buildings, principally because this sensing mode associates heights with scattering centres, thus giving rise to a more comprehensible and less cluttered scene. Fully Nyquist sampled 2D SAR apertures are difficult to collect however, so sparse trajectories were investigated. Sparse sampling of the 2D SAR aperture however, can give rise to image artefacts.

The classes of sparse trajectories investigated included repeat linear horizontal pass and a nonlinear height

separation variant, repeat crossing linear paths and a curved path variant and sinusoidal non-overlapping repeat passes.

For these classes of trajectories, the resolution of scattering centres can be thought of as mostly determined by the overall height and width extents of the trajectory ensemble, and the bulk of artefacts observed due to the sub-Nyquist sampling can be thought of as aliasing artefacts. In the extreme case where very little vertical resolution is observed, this viewpoint says that the vertical sidelobes are extreme aliased artefacts. These artefacts can be ejected from the image by increasing the density of sparse trajectories or they can be dimmed by spreading them across the image. Crossed trajectories spread the aliased artefacts, and the curved crossed trajectories even more so.

Non-overlapping sinusoid trajectories were observed to spread the aliased energy most, and given a required artefact free dynamic range, one can find a density of sinusoid trajectories to achieve this. It is stressed that this is not the case for linear repeat pass trajectories or even for the crossed trajectories, where the artefact free dynamic range is fixed even as the number of passes is increased, up until the trajectory density reaches the Nyquist sampling criterion and the aliased artefacts are ejected from the image.

For example, for the GBSAR dataset investigated, an artefact free dynamic range of approximately 15dB required 12 sinusoid trajectory passes, so that the vertical separation of passes is 12.5cm, which is substantially less than the 4.8cm separation required for the same or greater artefact free dynamic range with 32 repeat horizontal linear passes.

Further investigation will be conducted into the relationship of curved trajectory density and artefact free dynamic range, in order to achieve practical 2D SAR apertures for low frequency volumetric SAR imaging.

5.0 ACKNOWLEDGEMENTS

The authors wishes to thank Dr Francis Watson for interesting discussions on practical sparse trajectory options and Dstl for funding this research.

6.0 REFERENCES

[1] D. Andre, “An analysis of 3D SAR from single pass nonlinear radar platform trajectories”, Proceedings of SPIE - The International Society for Optical Engineering 7699, April 2010.

[2] D. Andre, B. Faulkner and M. Finnis “Low-frequency 3D synthetic aperture radar for the remote intelligence of building interiors”, IET Electronics Letters, 53 (15) 984-987, 2017

[3] D.A. Yocky, D.E. Wahl, C. V. Jakowatz, “Terrain elevation mapping results from airborne spotlight-mode coherent cross-track SAR stereo”, IEEE Transactions on Geoscience and Remote Sensing, Volume: 42, Issue: 2, Feb 2004